

RSC Advances



This is an *Accepted Manuscript*, which has been through the Royal Society of Chemistry peer review process and has been accepted for publication.

Accepted Manuscripts are published online shortly after acceptance, before technical editing, formatting and proof reading. Using this free service, authors can make their results available to the community, in citable form, before we publish the edited article. This *Accepted Manuscript* will be replaced by the edited, formatted and paginated article as soon as this is available.

You can find more information about *Accepted Manuscripts* in the [Information for Authors](#).

Please note that technical editing may introduce minor changes to the text and/or graphics, which may alter content. The journal's standard [Terms & Conditions](#) and the [Ethical guidelines](#) still apply. In no event shall the Royal Society of Chemistry be held responsible for any errors or omissions in this *Accepted Manuscript* or any consequences arising from the use of any information it contains.

1 **Zinc, copper and nickel derivatives of 2-[2-**
2 **bromoethyliminomethyl]phenol as topoisomerase inhibitors exhibiting**
3 **anti-proliferative and anti-metastatic properties**

4
5 Sze Koon Lee,^a Kong Wai Tan^{*a} and Seik Weng Ng^{a,b}

6
7 ^aDepartment of Chemistry, University of Malaya, 50603, Kuala Lumpur.

8 ^bChemistry Department, Faculty of Science, King Abdulaziz University, P. O. box
9 80203, Jeddah, Saudi Arabia.

10 (kongwai@um.edu.my)*

11
12
13 **Abstract**

14
15 Three transition metal derivatives of (2-[2-bromoethyliminomethyl]phenol),
16 $M[OC_6H_4CH=NCH_2CH_2Br]_2$ (M is zinc, copper and nickel) along with
17 $Ni[OC_6H_4CH=NCH_2CH_2]_2(H_2O)_4 \cdot 2Br$, were found to inhibit topoisomerase I (topo I)
18 activity, induce DNA cleavage and bind to calf thymus DNA. The compounds were
19 found to be cytotoxic when tested against cancer cell lines (A2780, MCF-7, HT29,
20 HepG2, A549, PC3, LNCaP), and were anti-invasive against PC3. The inhibitory
21 strength of the metal complexes was higher than that of the organic compound. The
22 neutral metal complexes were synthesized by reaction of the metal acetates with the
23 Schiff base ligand whereas the bromide salt was obtained upon recrystallization of the
24 nickel derivative from water. In the crystal structure of this salt, the cyclized Schiff
25 base ligand binds to the nickel atom through its nitrogen donor, the metal atom showing
26 an all-*trans* octahedral geometry. The metal atom in $Cu[OC_6H_4CH=NCH_2CH_2Br]_2$
27 exists in a square-planar environment.

28
29 **1. Introduction**

30
31 Camptothecin and its analogs target topoisomerase I¹, their activity being significantly
32 augmented upon complexation with metal ions^{2,3}. Researchers have addressed this
33 issue of metal-based drugs by using Schiff base complexes of zinc and copper⁴⁻⁷; for
34 example, Desideri and co-workers have proposed that the oxindole-Schiff base
35 complexes inhibit topo I activity through the interaction with amino acid residues at the
36 catalytic site of topo I⁶. Although other studies have explored the potential of Schiff
37 base complexes, by focusing on DNA interaction and cytotoxicity, topo I inhibition is
38 generally not examined⁸⁻¹¹.

39
40 Recently, two studies suggested that the corresponding derivatives of
41 thiosemicarbazones and hydrazones exhibit such behavior towards prostate cancer cells
42 (PC3)^{7,12}; the activity appears to be enhanced with the introduction of a bromoethyl
43 group¹³, the reason being attributed to the ability of the unit to alkylate the guanine
44 residues in DNA^{14,15}. Support for this is provided by Barton and co-workers, who
45 found that a rhodium intercalator tethered to an alkylating agent could selectively
46 alkylate mismatched DNA¹⁶.

47
48 With the above objectives in mind, we are reporting the syntheses and characterization
49 of $[Zn(L1)_2]$ (**1**), $[Cu(L1)_2]$ (**2**), $[Ni(L1)_2]$ (**3**), and $[Ni(L1^C)_2]$ (**4**) complexes (where
50 $L1^C$ is the self-cyclized **L1** ligand) of bromoethyl containing Schiff base (**L1**), as well as
51 their interaction with DNA and topoisomerase I, cytotoxic and anti-invasion activities
52 against the backdrop of their crystal structures.

53

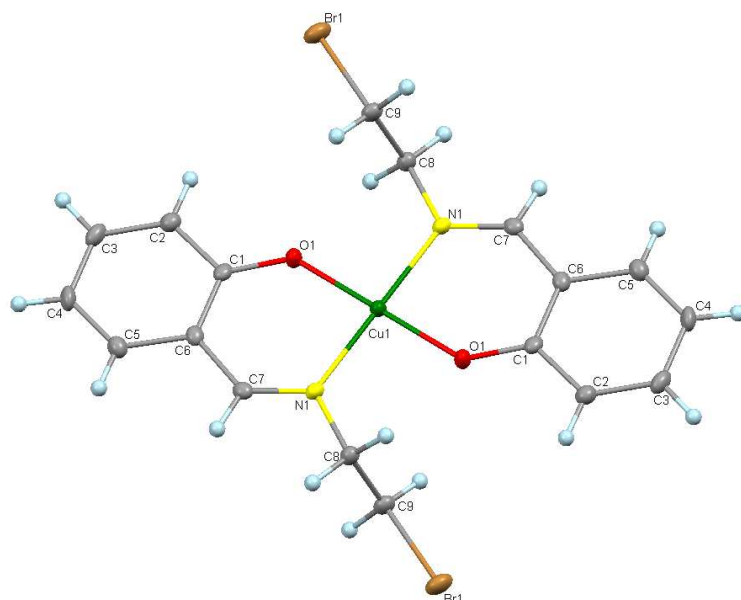
54 **2. Results and discussion**

55

56 **2.1 Crystal structure of Cu[OC₆H₄CH=NCH₂CH₂Br]₂**

57

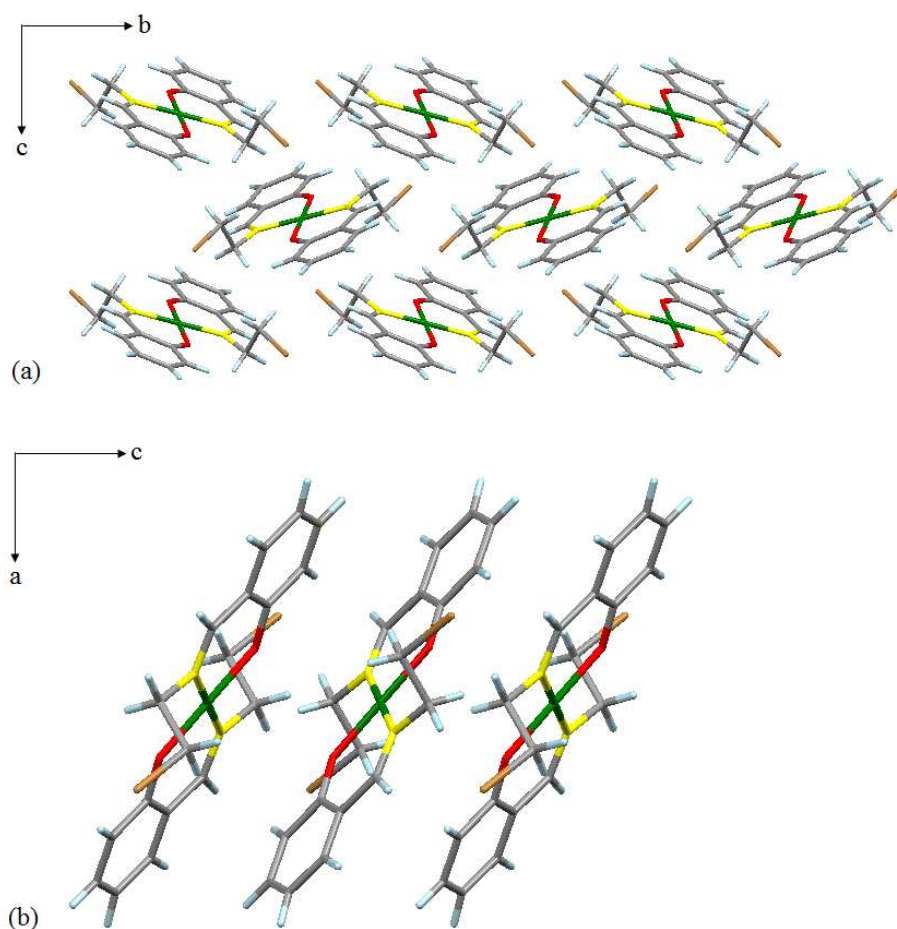
58 The crystal data and selected bond lengths and angles were presented in Table S1 and
59 S2 respectively. The metal atom in Cu[OC₆H₄CH=NCH₂CH₂Br]₂ (Fig. 1) is coordinated
60 by two phenolate oxygen atoms and two imine nitrogen atoms in an all-*trans* square
61 planar geometry. The Cu—O and Cu—N distances [1.896(2) Å and 2.008(2) Å] are in
62 good agreement with the bond distances found in other similar Schiff base complexes¹⁷,
63 ¹⁸. Molecules are stacked in a herringbone arrangement along the *a* axis (Fig. 2a) and
64 packed in a parallel fashion in the *b* projection (Fig. 2b).
65



66

67 **Fig. 1** Thermal ellipsoid plot of complex **2** is drawn at 50 % probability level. Hydrogen atoms are drawn
68 at arbitrary radii.

69



70
71 **Fig. 2** (a) The herringbone arrangement of complex **2** along the *a* axis. (b) The parallel packing of
72 complex **2** in the *b* projection. Green= Cu, red= O, yellow= N, brown= Br, grey= C, and blue= H
73

74 2.2 Spectroscopic measurements of L1 and complexes 1-4

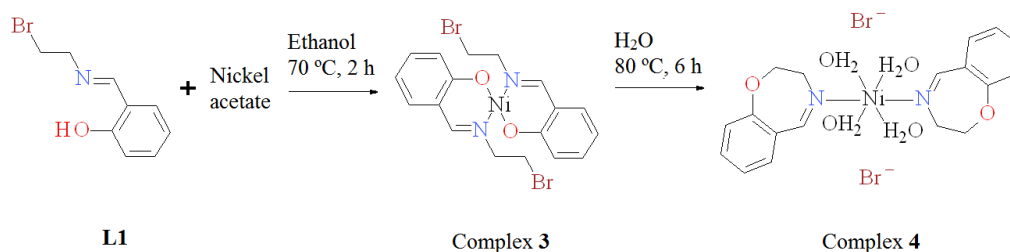
75
76
77 An intense band was observed in the range of 771-746 cm^{-1} in the IR spectra of **L1** and
78 complexes **1-3**, which is ascribed to the $\nu(\text{C-Br})$. Meanwhile, the $\nu(\text{C=N})$ of the
79 azomethine group in complexes **1-4** was shifted towards lower frequencies (1620-1606
80 cm^{-1}), indicating the coordination of imine nitrogen atom to the metal ions^{19,20}. Besides
81 that, the IR spectrum of complex **4** showed a sharp band at 3298 cm^{-1} assigned to the
82 $\nu(\text{OH})$ of coordinated water molecules.
83

84 Electronic spectra of **L1** and complexes **1-4** were recorded in DMSO in the region of
85 220-500 nm at room temperature. An intense absorption band at about 240-252 nm was
86 observed in **L1** and complexes **1-4** associated with the benzene ring $\pi-\pi^*$ transition²¹.
87 Besides that, Schiff base ligand **L1** has a characteristic absorption band at 397 nm ($\epsilon=$
88 $4.83 \times 10^3 \text{ M}^{-1} \text{ cm}^{-1}$) due to the $\pi-\pi^*$ transition of imine²². Upon complexation, the
89 absorption band of imine of complexes **2-4** has shifted to 373 nm ($\epsilon= 9.08 \times 10^3 \text{ M}^{-1} \text{ cm}^{-1}$),
90 361 nm ($\epsilon= 1.05 \times 10^4 \text{ M}^{-1} \text{ cm}^{-1}$), and 309 nm ($\epsilon= 2.74 \times 10^3 \text{ M}^{-1} \text{ cm}^{-1}$) respectively,
91 while the position of imine band of complex **1** remain unchanged at 397 nm ($\epsilon=$
92 $4.52 \times 10^3 \text{ M}^{-1} \text{ cm}^{-1}$). In addition, a broad band at 675 nm and 614 nm was observed for
93 complex **2** and complex **3** respectively, which were assigned to the d-d transition.
94 However, no d-d band was observed for complex **4**.
95

96 A characteristic peak assigned to the azomethine hydrogen at 8.3 ppm was observed,
 97 which confirmed the formation of Schiff base ligand **L1**. Aromatic protons of
 98 salicylaldehyde were present in the range of 6.88-7.48 ppm. The coordination of
 99 azomethine nitrogen to metal ion was supported by upfield shifting of CH=N peak from
 100 8.58 ppm in **L1** to 8.30 ppm in the spectrum of complex **1**^{23, 24}. In addition, the
 101 disappearance of the phenolic proton in the spectrum of complex **1** suggested the
 102 complexation of the ligand to metal ion *via* phenolate oxygen.
 103
 104

105 2.3 The reaction of complex **3** to form complex **4**

106
 107 Yet, what is particularly tantalizing is that the stirring of complex **3** in hot aqueous
 108 solution has catalyzed the self-cyclization of Schiff base ligand **L1** to obtain complex **4**
 109 with a seven-membered rings ligand (2,3-dihydro-1,4-benzoxazepine, **L1^C**) through
 110 Williamson ether reaction as shown in Fig. 3^{25,26}. However, the desired product could
 111 not be produced for complexes **1** and **2**. It is plausible that the self-cyclization of **L1** is
 112 catalyzed by the Ni(II) ions in the base free reaction. Similar observation was reported
 113 by Saha *et al.* recently in the synthesis of Ni(II) complex of 9-methoxy-2,3-dihydro-1,
 114 4-benzoxazepine, carried out in a different reaction condition²⁷. The conversion of **L1**
 115 to **L1^C** under such condition is notable as it involves green chemistry, achieves
 116 considerable yield, and relatively simple as compared to other reported methods²⁸⁻³¹.
 117



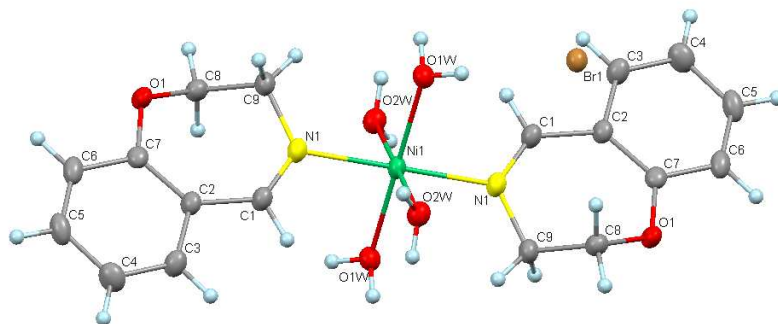
118
 119 **Fig. 3** Synthesis route of complex **4**.
 120
 121

122 2.4 Crystal structure of complex **4**

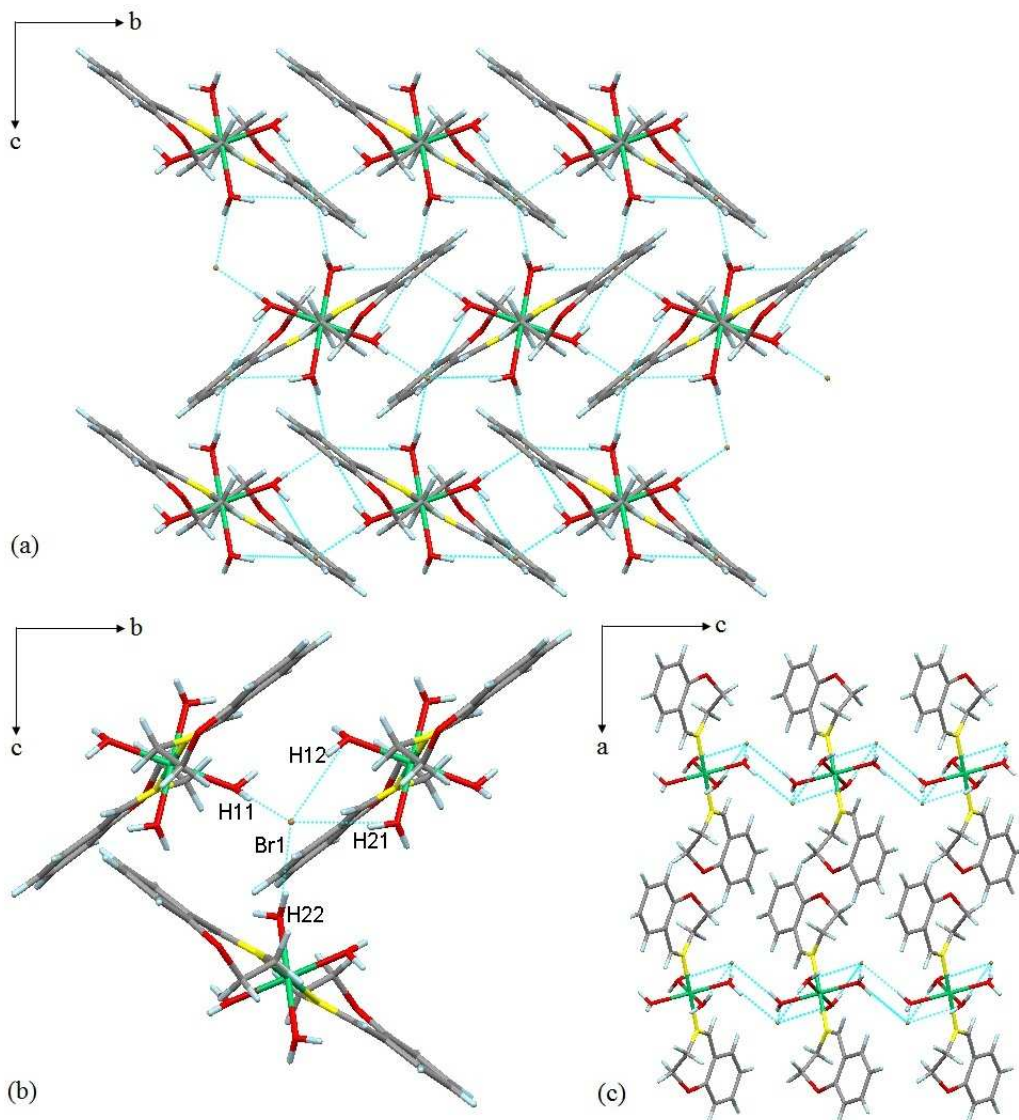
123
 124 The crystal data of complex **4** was tabulated in Table S1. Complex **4** crystallized in a
 125 monoclinic system and showed distorted octahedral environment since the angles of
 126 O1W-Ni1-O2W, N1-Ni1-O1W, and N1-Ni1-O2W are deviated from the ideal 90°. The
 127 nickel atom is ligated by two imine nitrogen atoms of two **L1^C** and four oxygen atoms
 128 of four water molecules (Fig. 4). Complex **4** is accompanied by two bromide anions due
 129 to its cationic nature. Both the coordinated **L1^C** are not planar due to the folding of
 130 seven-membered rings with O1, C8, and C9 out of the plane. The dihedral angles
 131 between the aromatic rings with C8-C9-N1 and O1-C7-C8 are 46.63° and 20.29°
 132 respectively. In addition, both the **L1^C** are trans to each other (N1-Ni1-N1 = 180°)^{32,33},
 133 the **L1^C** ligands are in the apical positions and four water molecules lie in the equatorial
 134 plane. The bond lengths of Ni1-N1, Ni1-O1W, and Ni1-O2W are 2.0778 (18) Å,
 135 2.0790 (18) Å, and 2.0879 (18) Å respectively, are matched well with the literature values²⁷
 136 (Table S2).
 137

138 The packing of the molecules of complex **4** is presented in Fig. 5. The aromatic rings
 139 are stacked in a herringbone fashion along the *a* axis. The distances of hydrogen
 140 bonding of complex **4** are shown in Table S3. The molecules in the crystal lattice are

141 stabilized by zigzag hydrogen bonding chains in *b* projection (Fig. 5c), a bromide anion
 142 is H-bonded with four H atoms of the coordinated water molecules (O1W—H11···Br1,
 143 O1W—H12···Br1, O2W—H21···Br1, and O2W—H21···Br1) and is responsible for the
 144 stacking arrangement (Fig. 5b).
 145



146
 147 **Fig. 4** Thermal ellipsoid plot of complex **4** is drawn at 50 % probability level. Hydrogen atoms are drawn
 148 at arbitrary radii.
 149



150
 151 **Fig. 5** (a) The herringbone packing of complex **4** in the *a* projection. (b) Hydrogen bonding between the
 152 water molecules and bromide anion. (c) The packing and hydrogen bonding pattern of complex **4** along

153 the *b* axis. Blue dotted lines represent hydrogen bonding. Green= Ni, red= O, yellow= N, brown= Br,
154 grey= C, and blue= H.

155

156

157 **2.5 Topoisomerase I inhibition assay**

158

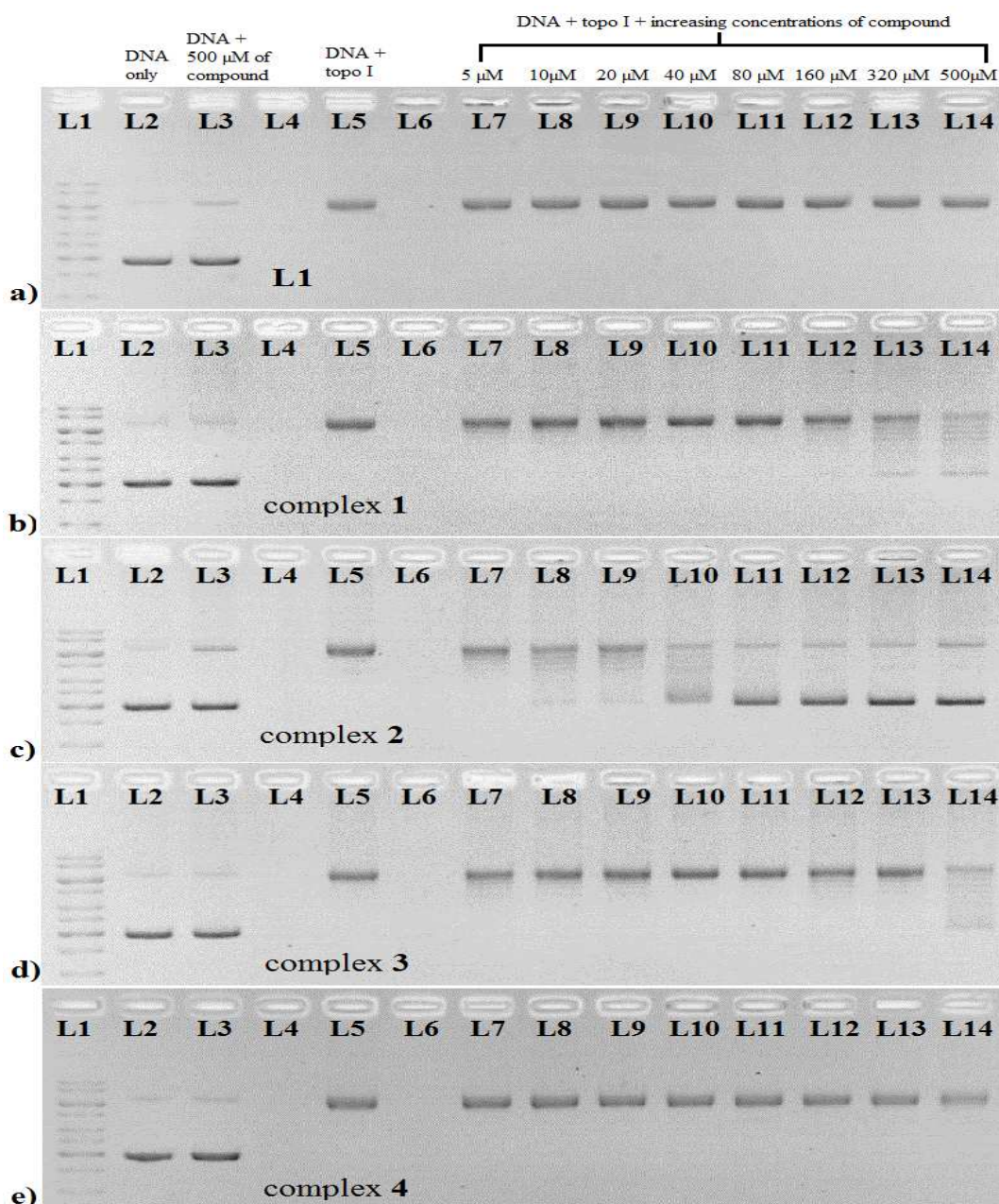
159 Complexes **1-3** inhibited the topo I activity in a dose dependent manner while **L1** and
160 complex **4** were found to be inactive as shown in Fig. 6. Complexation of **L1** has
161 enhanced the topo I inhibition effect^{2-4, 7, 13}. Cu(II) complex **2** was the most active
162 complex in this series, since partial inhibition of topo I activity was induced at 10 μM
163 and total inhibition was observed at 80 μM . On the other hand, Zn(II) complex **1** and
164 Ni(II) complex **3** required a higher concentration, 250 μM and 500 μM respectively to
165 induce slight inhibition of topo I activity. No complete inhibition was detected for
166 complexes **1** and **3**. The appearance of DNA laddering in the gel suggested that
167 complexes **1-3** may act as topo I poisons by stabilizing the DNA-topo I cleavage
168 complex⁵. The inhibitory strength of these compounds was found to follow the order: **2**
169 $> \mathbf{1} > \mathbf{3} > \mathbf{4} \approx \mathbf{L1}$.

170

171 According to Desideri *et al.*, oxindolimine Zn(II) and Cu(II) complexes could inhibit
172 topo I activity, with the Cu(II) complex being more active than the Zn(II). The
173 molecular docking study showed that this difference is due to the different coordination
174 geometry of the complexes. The square planar Cu(II) complex formed a stable complex
175 with amino acid residues of topo I in one of the two “lips” that clamp DNA during the
176 cleavage reaction, whereas the more tetrahedral Zn(II) complex only allowed a loose
177 interaction with topo I⁶. This may also explains why the octahedral complex **4** with
178 non-planar ligands is inactive in inhibiting topo I activity.

179

180



181
 182 **Fig.6** Electrophoresis result of incubating *E. coli* topo I (0.25 unit/20 μl) with pBR322 in the absence and
 183 presence of various concentrations (5-500 μM) of **L1** (a), **1** (b), **2** (c), **3** (d), and **4** (e). Lane 1, Gene
 184 Ruler™ 1 kb DNA ladder; lane 2, DNA alone; lane 3, DNA + 500 μM of **L1** or **1-4**; lane 5, DNA + 0.25
 185 unit *E. coli* topo I; lane 7-14, DNA + 0.25 unit *E. coli* topo I + increasing concentrations of **L1** or **1-4** (5
 186 μM, 10 μM, 20 μM, 40 μM, 80 μM, 160 μM, 250 μM, and 500 μM respectively).
 187

188 2.6 Nucleolytic study

189
 190 We observed that the **L1** exhibits comparable DNA cleavage activity with its metal
 191 complexes in the absence of external agent at neutral pH, while metal chloride alone has
 192 a negligible effect on DNA cleavage as shown in Fig. 7. Schiff base ligand **L1** and
 193 complexes **1-3** started to induce double-stranded DNA scission with different
 194 concentration of 80 μM, 40 μM, 20 μM, and 160 μM respectively. In addition, **L1**,
 195 complexes **1** and **2** were able to cut linear DNA into smaller fragments that cannot be
 196 quantified at 500 μM-1 mM, causing smearing and fading of DNA bands. On the other
 197 hand, complex **4** was a relatively weaker but site specific nucleolytic agent as it

198 catalyzed the cleavage reaction and produced 23.5-27.4 % of nicked DNA at a variety
199 of concentrations (5-250 μM), and restrained the migration of DNA across the gel
200 starting from 500 μM ; suggestive of binding of complex **4** to DNA forming DNA
201 aggregates. This might be due to the difference in structure and coordination geometry
202 of complex **4**. Result showed that these compounds cleaved DNA by the following
203 order: **2** > **1** > **L1** > **3** > **4** based on their ability to catalyze the cleavage reaction to
204 produce linear DNA at 80 μM .

205

206 It is not surprising that Schiff base ligand **L1** can perform DNA scission. There are
207 several studies reporting better DNA cleavage activity of the free ligand than its Co (II)
208 and Zn(II), Cu(II), and Ni(II) complexes³⁴⁻³⁶. The phenyl ring of **L1** may intercalate
209 into DNA, while the hydroxyl group acts as a nucleophilic group in the
210 transphosphorylation reaction^{34, 36-39}. Nevertheless, the significant DNA cleavage
211 activity induced by **L1** is probably due to its smaller molecular size and lack of any site
212 specificity as compared to its tetra-coordinated metal complexes. The DNA cleavage
213 activity of complexes **1-3** is reminiscent of the Schiff base **L1**, demonstrating the role of
214 ligand in the DNA cleavage mechanism.

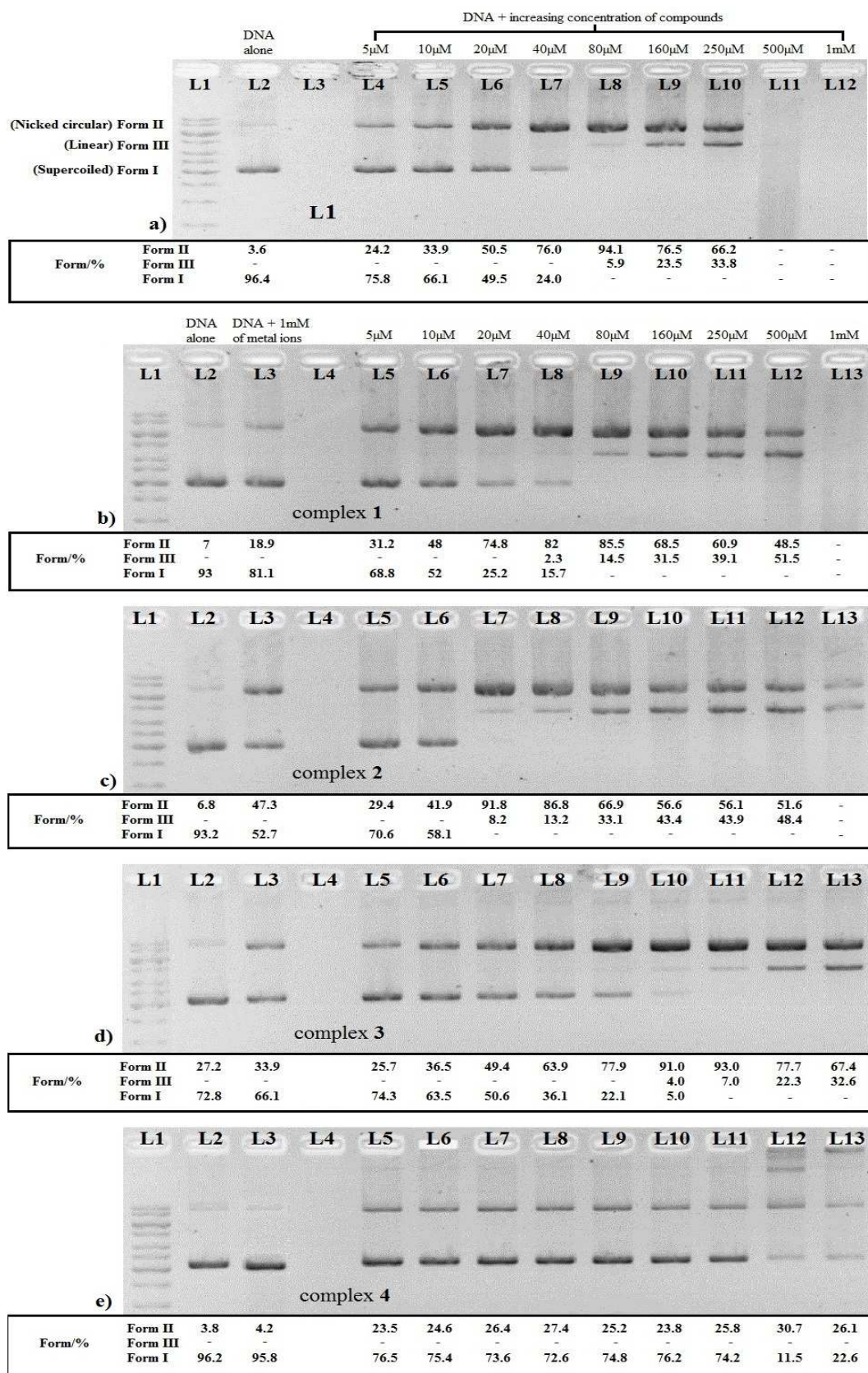
215

216 Even though the DNA cleavage reaction of Cu(II) and Ni(II) complexes **2-4** does not
217 require external agent, the possibility that DNA cleavage occurs *via* the production of
218 reactive oxygen species (ROS) need to be discounted; so mechanistic study using
219 scavengers of hydroxyl radical (DMSO and thiourea), singlet oxygen radical (sodium
220 azide), and superoxide anion (tiron), and a Cu(I) specific chelator (neocuprione) were
221 carried out (Fig. S1). For Cu(II) complex **2**, the addition of neocuprione had partially
222 inhibited the DNA cleavage; with the retainment of supercoiled DNA (40.1 %).
223 Moreover, thiourea, sodium azide, and DMSO reduced the conversion of nicked DNA
224 to linear DNA by 8-10 %. All of the above results corroborated a self-activating
225 mechanism for complex **2**; whereby the redox-active Cu(II) center is initially reduced to
226 Cu(I), and subsequently reacts with dioxygen to produce hydroxyl and singlet oxygen
227 radicals that cause the DNA breaks^{40, 41}, thus, the involvement of oxidative pathway in
228 the cleavage reaction catalyzed by complex **2** cannot be ruled out. However, a rare
229 phenomenon was observed where the addition of tiron enhanced the DNA cleavage
230 activity by producing 49.1 % linear DNA, the exact reason is still under investigation
231 and similar observation has been reported by Seng *et al*⁴². Furthermore, thiourea caused
232 smearing above the nicked DNA band that contains a variety of DNA conformations,
233 which might be due to the binding of complex **2** on the partially-catalyzed cleaved
234 residues of nicked DNA. On the other hand, all of the tested radical scavengers have no
235 obvious effect on the extent of DNA cleavage by Ni(II) complexes **3** and **4**. It is not
236 uncommon for Cu(II) and Ni(II) complexes to carry out DNA cleavage in the absence
237 of external agent^{43, 44}.

238

239

240



241
242
243
244
245
246

Fig. 7 Electrophoresis result of incubating pBR322 with **L1** (a), **1** (b), **2** (c), **3** (d), and **4** (e) in TN buffer (5 mM Tris, 50 mM NaCl) pH 7.5 at 37 °C for 48 h. Lane 1, Gene Ruler™ 1 kb DNA ladder; lane 2, DNA alone; lane 3 (7b-7e), DNA + 1 mM MCl₂ (M= Zn, Cu, Ni); lane 4-12 (7a), DNA + increasing concentrations of **L1** (5 μM- 1 mM); lane 5-13 (7b-7e), DNA + increasing concentrations of **1-4** (5 μM- 1 mM respectively).

247

248 **2.7 DNA binding study**

249

250 The absorption spectra of **L1** and complex **1** incubated with increasing CT-DNA
 251 concentrations are shown in Fig. 8, while the absorption spectra of complexes **2-4** are
 252 shown in Fig. S2. Schiff base ligand **L1** and complexes **1-3** exhibited different degree of
 253 hypochromism at 361-397 nm, accompanied by a blue shift as tabulated in Table 1.
 254 Besides that, slight hyperchromism at ~320 nm and the appearance of an isobestic point
 255 at 330-350 nm upon the addition of CT-DNA for **L1**, complexes **1** and **3** suggested the
 256 existence of an equilibrium between the free compound and CT-DNA bound
 257 compound. On the other hand, complex **4** showed modest hypochromism (5.79 %) at
 258 309 nm. The observed hypochromism and blue shift may be an evidence of non-
 259 covalent interaction between the compounds and DNA; probably *via* intercalation⁴⁵⁻⁴⁸.

260

261 Complex **1** exhibits highest K_b value (3.62×10^7), followed by **L1** (1.07×10^7), **4**
 262 (6.68×10^6), **3** (5.22×10^6), and **2** (8.20×10^5). The K_b values of **L1** and complexes **1-4** are
 263 comparable to classical intercalator ethidium bromide ($1.4 \times 10^6 \text{ M}^{-1}$)⁴⁹ and
 264 metallointercalator $[\text{Ru}(\text{bpy})_2(\text{dppz})]^{2+}$, bpy= 2,2'-bipyridine, dppz= dipyrrodo[3,2-
 265 a:2',3'-c]phenazine) ($> 10^6 \text{ M}^{-1}$)^{50, 51}. Furthermore, similar trend was observed in the
 266 interaction of metallopyrazoliumylporphyrins with CT-DNA, the K_b values followed
 267 the trend $\text{Zn} > \text{Ni} > \text{Cu}$, probably due to different interaction mode and preferential
 268 DNA-sequence affinity^{52, 53}.

269

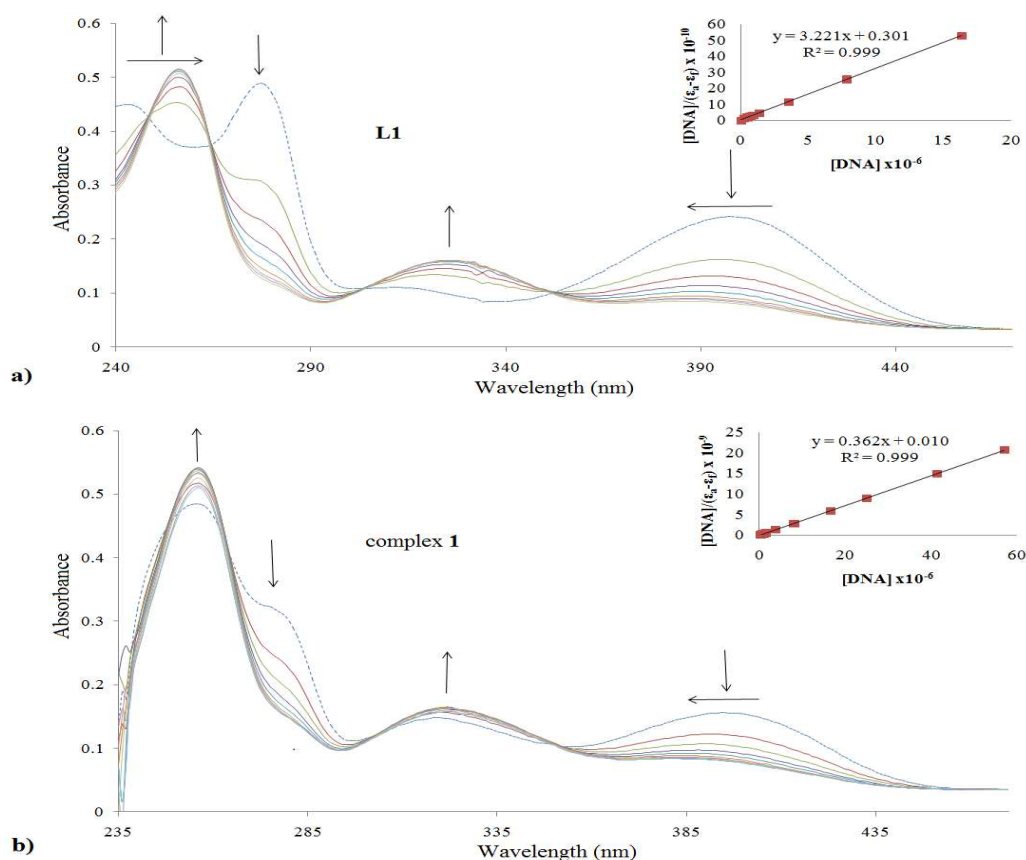
270

271 **Table 1** Spectral features of the UV spectra of **L1** and complexes **1-4** upon addition of CT-DNA.

Compound	λ (nm)	Change in absorbance	Isobestic point (nm)	Red shift (nm)	Blue shift (nm)	Hypo (%)	K_b/M^{-1}
L1	397	Hypochromism	352	-	19	64.65	1.07×10^7
1	397	Hypochromism	351	-	14	62.83	3.62×10^7
2	373	Hypochromism	-	-	21	46.61	8.20×10^5
3	361	Hypochromism	335	-	5	51.08	5.22×10^6
4	309	Hypochromism	-	-	-	5.79	6.68×10^6

272

273



274
 275 **Fig. 8** UV-Vis absorption spectra of **L1** (a) and **1** (b) in TN buffer pH 7.5, in the absence (dashed line)
 276 and presence (solid line) of CT-DNA with increasing concentrations. Arrows show the change in
 277 absorbance with increasing DNA concentration. The insets represent the K_b calculation plots for the
 278 spectra changes at 397 nm of **L1** and complex **1**.
 279

279

280

281 2.8 Cytotoxicity study

282

283 The cytotoxic activity of Schiff base ligand **L1** and complexes **1-4** against various
 284 human cancer cell lines such as A2780, MCF-7, HT29, HepG2, A549, PC3, and LNCaP
 285 were evaluated by MTT assay and presented in Table 2. Cultured cancer cells were
 286 treated with compounds and incubated for 24 h and the IC_{50} values were determined
 287 from the plots of cancer cells survival against increasing concentration of tested
 288 compounds as shown in Fig. S3 and S4. Cisplatin was used as a positive control. Schiff
 289 base ligand **L1** and complex **4** were inactive in all the cell lines tested, whereas complex
 290 **3** was relatively less cytotoxic to cancer cells than complexes **1** and **2**. The
 291 complexation of **L1** with Zn(II) and Cu(II) metal ions greatly enhanced its cytotoxic
 292 activity. Zn(II) complex **1** displayed significant cytotoxic activity towards PC3 and
 293 LNCaP cells ($<15 \mu\text{M}$), while Cu(II) complex **2** was highly toxic against HT29, HepG2,
 294 PC3, and LNCaP ($<20 \mu\text{M}$). It is not astonishing that complex **1** exerts prominent
 295 cytotoxic activity against prostate cancer cells because human prostate epithelial cells
 296 are shown to uniquely accumulate high level of zinc and consequently induce apoptotic
 297 cell death^{54, 55}.
 298

298

299 Moreover, this finding is consistent with the result from topo I inhibition study as
 300 shown in Fig 6. The level of topo I is often overexpressed in colon, lung, and prostate
 301 cancers⁵⁶. Complex **2** being the most active topo I inhibitor in this series also exhibits

302 remarkable cytotoxic activity against these cancer cell lines, which proposed that
303 complexes **1-3** induced cytotoxicity by inhibiting topo I activity.

304

305

306 **Table 2** Cytotoxic activity of Schiff base **L1** and its metal complexes **1-4** against several cancer cell lines
307 after 24 h treatment.

Compound	IC ₅₀ (μM)						
	A2780 Ovarian cancer	MCF-7 Breast cancer	HT29 Colon cancer	HepG2 Hepatocellular carcinoma	A549 Lung carcinoma	PC3 Prostate carcinoma	LNCaP
Cisplatin	28.80	19.60	25.00	152.00	35.40	271.50	32.53
L1	>80	>80	>80	>80	>80	>80	>80
1	68.97	26.77	32.83	67.60	>80	14.93	13.60
2	70.70	25.77	14.07	18.47	29.43	17.37	14.10
3	>80	>80	68.02	>80	61.77	57.77	41.70
4	>80	>80	>80	>80	>80	>80	>80

308

309

310 **2.9 Cell invasion study**

311

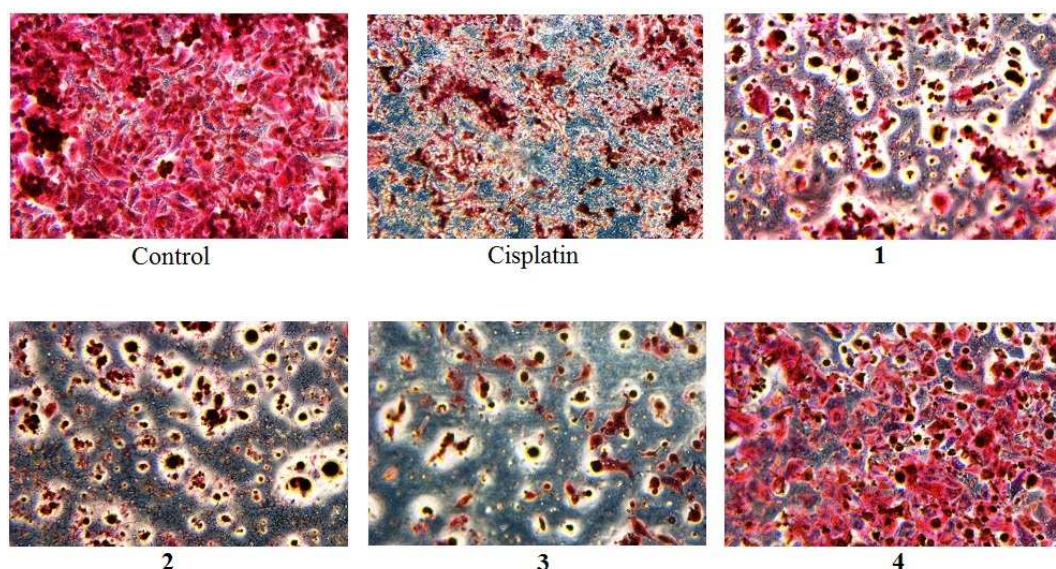
312 The metastasis of cancer cells to remote sites is the major cause of cancer death^{57, 58}.
313 Cancer cells will need to degrade the basement membrane before they spread and
314 invade through the body. Therefore, the cell invasion assay employs the protein
315 complex Matrigel, which simulates the *in vivo* cellular basement membrane and
316 demonstrates the anti-invasive activity of compounds by keeping the cancer cells
317 localized. The lesser the number of cancer cells migrate through the Matrigel, the
318 greater the ability of compound to prevent the invasion of cells⁵⁹. Since most of the
319 tested compounds were active against prostate cancer, we decided to study the anti-
320 invasive activity of these compounds on the more invasive PC3 cancer cells^{60, 61}. The
321 result obtained from the study was depicted in Fig. 9 and 10.

322

323 The invasion rates of PC3 cells after treated with cisplatin and complexes **1-4** were
324 47.79± 16.62 %, 24.87± 8.33 %, 14.97± 13.32 %, and 7.78± 9.54 %, and 80.86±
325 18.18 % respectively (invasion rates are normalized over the control). Notably,
326 complexes **1-3** were quite effective anti-invasive agents as compared to complex **4** and
327 cisplatin. Counterintuitively, the less cytotoxic complex **3** has created a greater obstacle
328 for the invading cells than the more cytotoxic complexes **1** and **2**. It is not surprising as
329 the ruthenium compound, imidazolium *trans*-imidazoledimethyl sulfoxidetetrachloro-
330 ruthenate (NAMI-A) also shows similar characteristics^{62, 63}. Based on the result
331 obtained, it was proposed that the Ni(II) complex exhibits better anti-invasion activity
332 against PC3 cells than its Zn(II) and Cu(II) analogs, but the absence of bromoalkyl
333 group significantly reduced the activity as shown by Ni(II) complex **4**. Recently,
334 Radulovic and colleague showed a rare example of Ni(II) complex of
335 selenosemicarbazones that could inhibit the invasion of human breast cancer MDA-
336 MB-361 cells more effectively than the Cd(II) and Zn(II) complexes⁶⁴.

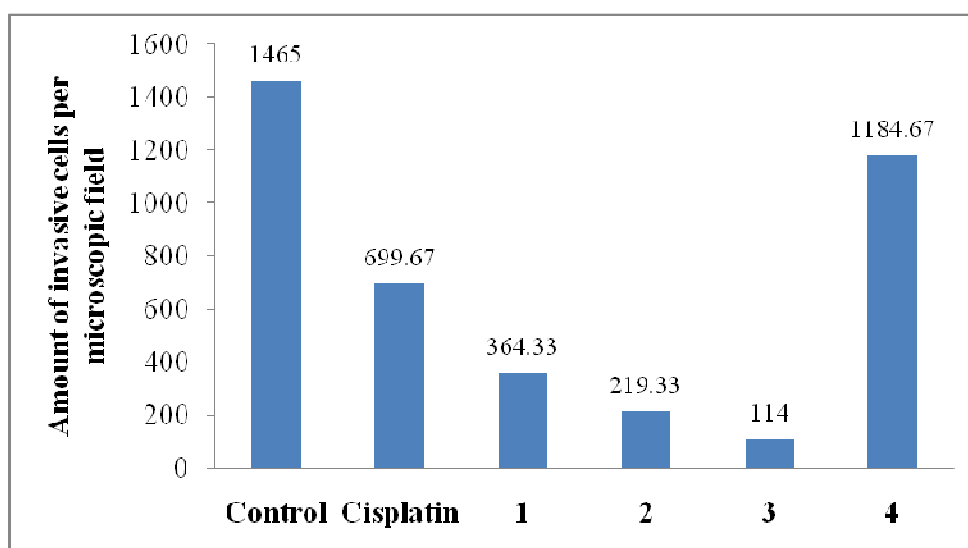
337

338



339
340
341
342
343
344

Fig. 9 Microscope images of invading PC3 cells that have migrated through the Matrigel: The extent of inhibition of cell invasion by cisplatin and complexes 1-4 against PC3 cells can be seen from the decrease in the numbers of invading cells.



345
346
347
348

Fig. 10 Cell invasion assay result of cisplatin and complexes 1-4 against PC3.

3. Experimental

3.1 Materials and solutions

352
353
354
355
356
357
358
359
360
361

The chemicals for syntheses were bought from Sigma and solvents were purchased from Merck. The pBR322, gene ruler 1kb DNA ladder, 6x loading buffer, were purchased from BioSyn Tech (Fermentas). Analytical grade agarose powder was bought from Promega. *E. coli* topoisomerase I was purchased from New England Biolabs. Calf-thymus DNA (CT-DNA), sodium chloride, and ethidium bromide were bought from Sigma Chemical Co. (USA). All solutions for DNA experiments were prepared with ultra-pure water from an Elga PURELAB ULTRA Bioscience water purification system with UV light accessory. Tris-NaCl (TN) buffer was prepared from the combination of Tris base and NaCl dissolved in aqueous solution. The pH of TN buffer was adjusted

362 with hydrochloric acid solution until pH 7.5, which contains Tris at 5 mM and NaCl at
363 50 mM. All the tested compounds were freshly prepared daily.

364

365

366 3.2 Physical measurements

367

368 IR spectra were recorded as KBr pellets by using a Perkin-Elmer Spectrum RX-1
369 spectrometer. NMR spectra were recorded in deuterated DMSO-d on a JEOL JNM-
370 LA400 or ECA 400 MHz instrument. Elemental analyses were carried out on a Thermo
371 Finnigan Eager 300 CHNS elemental analyzer. UV-Vis spectroscopic measurements
372 were performed on a Shimadzu UV-1650 PC spectrophotometer.

373

374

375 3.3 Syntheses

376

377 3.3.1 Synthesis of 2-[2-bromoethyliminomethyl]phenol (L1)

378

379 The Schiff base ligand **L1** was synthesized according to the method described by
380 Grivani *et al.* with minor modification²⁰. Rapid evaporation of the solvent yielded
381 yellow needle crystals in high yield. The crystals were filtered, washed with water, dried
382 in the air, and kept in a desiccator over silica gel.

383

384 (Yield: 1.87 g, 82 %). Anal. Calc. for C₉H₁₀BrNO: C, 47.4; H, 4.4; N, 6.1. Found: C,
385 47.2; H, 4.3; N, 6.3. IR (KBr disc, cm⁻¹): 3005 w, 2883 m, 2832 w, 2725 w, 2654 w,
386 1630 s (C=N), 1498 m, 1429 m, 1277 s, 1264 s, 1056 s, 841 s, 760 s (C-Br), 639 m, 560
387 m, 454 m (s, strong; m, medium; w, weak).

388

389 Characteristic ¹H NMR signals (DMSO-*d*₆, TMS, s, singlet; d, doublet; m, multiplet) δ
390 (ppm): 13.21 (s, 1H, O-H), 8.58 (s, 1H, H-C=N), 6.88-7.48 (m, 4H, C-H, phenyl), 4.00
391 (d, 2H, N-CH₂-), and 3.80 (d, 2H, -CH₂Br).

392

393

394 3.3.2 Synthesis of [Zn(L1)₂] (1)

395

396 **L1** (0.46 g, 2 mmol) was added dropwise into an ethanolic solution of zinc acetate (0.22
397 g, 1 mmol) and refluxed for 2 h. Yellow precipitates formed were filtered, washed with
398 ethanol and water, dried in the air, and kept in a desiccator over silica gel.

399

400 (Yield: 0.31 g, 68 %). Anal. Calc. for C₁₈H₂₀Br₂N₂O₂Zn: C, 41.5; H, 3.9; N, 5.4. Found:
401 C, 41.6; H, 3.3; N, 5.5. IR (KBr disc, cm⁻¹): 3435 W, 3032 w, 2955 w, 1620 s (C=N),
402 1537 s, 1467 m, 1450 m, 1324 m, 1189 m, 1148 m, 757 m (C-Br), 598 w, 465 w, 450 w
403 (s, strong; m, medium; w, weak).

404

405 Characteristic ¹H NMR signals (DMSO-*d*₆, TMS, s, singlet; d, doublet; m, multiplet) δ
406 (ppm): 8.3 (s, 2H, H-C=N), 6.88-7.48 (m, 8H, C-H, phenyl), 4.00 (d, 4H, N-CH₂-), and
407 3.81 (d, 4H, -CH₂Br).

408

409

410 3.3.3 Synthesis of [Cu(L1)₂] (2)

411

412 The general procedure for the synthesis is similar to the complex **1** by using copper
413 acetate to replace zinc acetate. Green crystals suitable for X-ray diffraction study were

414 obtained by dissolving the green powders in a mixture of dimethylformamide and
415 ethanol and allowed to evaporate slowly at room temperature.

416

417 (Yield: 0.37 g, 72 %). Anal. Calc. for $C_{18}H_{20}Br_2N_2O_2Cu$: C, 41.6; H, 3.9; N, 5.4. Found:
418 C, 41.8; H, 3.3; N, 5.3. IR (KBr disc, cm^{-1}): 3024 w, 2908 w, 1611 s (C=N), 1443 s,
419 1326 s, 1204 m, 1150 m, 908 m, 749 s (C-Br), 733 s, 677 s, 610 m, 577 m, 466 m (s,
420 strong; m, medium; w, weak).

421

422

423 3.3.4 Synthesis of $[Ni(L1)_2]$ (3)

424

425 The general procedure for the synthesis is similar to the complex **1** by using nickel
426 acetate to replace zinc acetate. Pale green precipitates formed were filtered, washed with
427 water and ethanol, and kept in a desiccators over silica gel.

428

429 (Yield: 0.39 g, 75 %). Anal. Calc. for $C_{18}H_{20}Br_2N_2O_2Ni$: C, 42.0; H, 3.9; N, 5.4. Found:
430 C, 42.0; H, 3.4; N, 5.4. IR (KBr disc, cm^{-1}): 3437 w, 3029 w, 2935 w, 1610 s (C=N),
431 1539 s, 1336 m, 1224 m, 1148 m, 917 s, 746 m (C-Br), 733 m, 639 m, 533 m, 462 m,
432 411 m (s, strong; m, medium; w, weak).

433

434

435 3.3.5 Synthesis of $[Ni(L1^C)_2]$ (4)

436

437 Complex **3** (0.515 g, 1 mmol) was stirred in 20 ml of hot water and it was slowly
438 dissolved over 6 h. Then, the aqueous solution was concentrated to 5 ml and slow
439 evaporation at room temperature yielded green crystals suitable for X-ray analysis. The
440 green crystals were filtered, washed with diethyl ether and kept in a desiccator over
441 silica gel.

442

443 (Yield: 0.362 g, 62 %). Anal. Calc. for $[(C_9H_9NO)(H_2O)_4Ni]^{2+} \cdot 2Br^-$: C, 37.0; H, 4.5; N,
444 4.8. Found: C, 37.2; H, 4.4; N, 5.1. IR (KBr disc, cm^{-1}): 3298 s, 2972 w, 2927 w, 1644
445 s, 1606 s (C=N), 1564 m, 1491 m, 1273 s, 1181 m, 1128 m, 1060 m, 979 s, 871 w, 771 s
446 (C-Br), 700 w, 661 w, 603 w, 575 w, 509 s (s, strong; m, medium; w, weak).

447

448

449 3.4 X-ray crystallography

450

451 The unit cell parameters and the intensity data were collected on a Bruker SMART
452 APEX diffractometer, equipped with a Mo-K α X-ray source ($\lambda = 0.71073 \text{ \AA}$). The
453 APEX2 software was used for data acquisition and the SAINT software for cell
454 refinement and data reduction. Absorption corrections on the data were made using
455 SADABS. The structures were solved and refined by SHELXL97⁶⁵. Molecular
456 graphics were drawn by using XSEED⁶⁶. The structures were solved by direct-methods
457 and refined by a full-matrix least-squares procedure on F^2 with anisotropic displacement
458 parameters for non-hydrogen atoms.

459

460 Crystallographic data for the structural analysis have been deposited with the
461 Cambridge Crystallographic Data Center, CCDC 1007051 for complex **2** and CCDC
462 1007052 for complex **4**. Copies of the information may be obtained free of charge from
463 the director, CCDC, 12 Union Road, Cambridge, CB2, IEZ, UK, (fax: +44-1223-336-
464 033; E-mail: deposit@ccdc.cam.ac.uk or <http://www.ccdc.cam.ac.uk>).

465

466

467 **3.5 *E. coli* topo I inhibition assay**

468

469 The *E. coli* topo I inhibitory activity was determined by observing the relaxation of
470 supercoiled plasmid DNA, pBR322. The reaction mixtures for this test consisted of 1x
471 BSA, 10x NE buffer 4, 0.25 μg of plasmid pBR322, 0.25 units of *E. coli* topo I, and
472 compounds with final concentration of 500 μM . All reactions conducted at a final
473 volume of 20 μl and were prepared on ice. Upon enzyme addition, reaction mixtures
474 were incubated at 37 $^{\circ}\text{C}$ for 30 mins. The reactions were terminated by adding 2 μl of
475 10 % sodium dodecyl sulfate (SDS) and followed by 3 μl of 6x loading dye comprising
476 0.03 % bromophenol blue and 60 % glycerol. SDS is required to observe a linear DNA
477 fragment and to denature topo I, preventing further functional enzymatic activity. Then,
478 the reaction mixtures were loaded into 1.25 % agarose gel and electrophoresed for 3 h at
479 50 V with running buffer of Tris-acetate EDTA (TAE) at pH 8.1. The gel was stained,
480 destained, and photographed under UV light using an AlphaImager red[®] gel
481 documentation system and the digital image was analyzed using Pronto software.

482

483

484 **3.6 DNA cleavage experiment**

485

486 Agarose gel electrophoresis experiments were performed on supercoiled plasmid DNA
487 pBR322 using a horizontal gel system. For the cleavage studies, each 20 μl of sample
488 contained the compound dissolved in buffer, DNA, and the required volume of
489 additional buffer. All samples were incubated at 37 $^{\circ}\text{C}$ in the dark. The reaction
490 mixtures were prepared as follows: 0.5 μl of 50 μM compound or metal salt was added
491 to the mixture of 0.5 μl of plasmid DNA pBR322 (0.25 $\mu\text{g}/\mu\text{l}$) and Tris-NaCl buffer at
492 pH 7.5 to give a final volume of 20 μl . The reactions were carried out after incubating
493 the reaction mixtures at 37 $^{\circ}\text{C}$ for 48 h. Next, 3 μl of 6x loading dye was added to the
494 reaction mixtures and electrophoresed at 80 V for 90 mins in Tris-acetate-EDTA (TAE)
495 buffer, pH 8.1, using 1.5 % agarose gel. Then, the agarose gel was stained with
496 ethidium bromide solution (0.5 $\mu\text{g}/\text{ml}$). Densitometric quantification of supercoiled
497 DNA and cleavage products after electrophoresis was estimated using TotalLab Quant
498 software^{34, 67}. Supercoiled plasmid DNA values were corrected by a factor of 1.3 due to
499 the lowered binding of ethidium to this structure⁶⁸⁻⁷⁰. To study the DNA cleavage
500 mechanism, several radical scavengers (Tiron, thiourea, DMSO, and sodium azide) and
501 a specific Cu(I) chelator (neocuprione) were used⁴². The reaction mixtures were
502 incubated at 37 $^{\circ}\text{C}$ for 24 h.

503

504

505 **3.7 DNA binding study with UV spectroscopy**

506

507 DNA binding studies have been performed by UV-vis spectroscopic titration using TN
508 buffer (5 mM Tris; 50 mM NaCl, pH 7.5) at room temperature. Stock solutions of tested
509 compounds were prepared in DMSO and diluted with TN buffer to a concentration of
510 50 μM as working solutions in the titration experiments. The final concentration of
511 DMSO in the working solution was not more than 10 %. DNA stock solution was
512 prepared by dissolving the commercially purchased CT-DNA in TN buffer at 4 $^{\circ}\text{C}$ for 2
513 days. The purity of the CT-DNA stock solution was checked by comparing the ratio of
514 absorbance at 260 nm and 280 nm. The DNA concentration was determined by the UV
515 absorbance at 260 nm after 1:10 dilution using a molar extinction coefficient at 6600 M^{-1}
516 cm^{-1} . CT-DNA stock solution was added gradually into the reaction mixture up to a
517 sufficient concentration for studying. After each addition, the reaction mixture was

518 allowed to incubate for 5 mins before the absorption spectrum was recorded. The
519 intrinsic binding constant K_b of tested compounds were calculated by using the Wolfe-
520 Shimmer equation:^{71, 72}

$$521 \\ 522 \quad [DNA]/(\epsilon_a - \epsilon_f) = [DNA]/(\epsilon_b - \epsilon_f) + 1/K_b (\epsilon_b - \epsilon_f)$$

523
524 where ϵ_a , ϵ_f , and ϵ_b correspond to $A_{\text{obsd}}/[\text{compound}]$, the extinction coefficient for the
525 free compounds, and the extinction coefficient for the compounds fully bound with
526 DNA. In plot of $[DNA]/(\epsilon_a - \epsilon_f)$ versus $[DNA]$, the intrinsic binding constant K_b is given
527 by the ratio of the slope to y-intercept.

528

529

530 **3.8 Cytotoxicity assay**

531

532 Cells used in this study were obtained from American Type Cell Collection (ATCC)
533 and Lonza. These tumour cells were cultured in a RPMI 1640 medium at 37 °C in an
534 atmosphere with 5 % CO₂ saturation. *In vitro* cytotoxicity for quantitative evaluation
535 was tested by means of the MTT assay. Cells were seeded at a density of 1 x 10⁵ cells/
536 ml in a 96-well plate and incubated for 24 h. On the next day, the tested compounds
537 were dissolved in DMSO and added to the wells. DMSO was used as the vehicle control.
538 After 24 h of incubation at 37 °C, 20 µl of MTT solution was added to each well and the
539 plates were incubated for 2 h. The purple formazan formed was dissolved by the
540 addition of 100 µl of DMSO to each well. Absorbance at 580 nm was measured and
541 recorded using a 96-well microplate reader. The potency of cell growth inhibition for
542 each test agent was expressed as an IC₅₀ value, which defined as the concentration that
543 caused 50 % inhibition of cell growth.

544

545

546 **3.9 Cell invasion study**

547

548 The BD BioCoat™ Matrigel™ invasion chamber (BD Biosciences) was used according
549 to the manufacturer's instructions. Compounds were dissolved in cell media at the
550 desired concentration and dissolved in Matrigel. Twenty-five thousand of prostate
551 cancer cells (PC-3) in serum free media were then seeded in the top chamber of the two-
552 chamber Matrigel system. To the lower compartment, RPMI/5 % FCS was added as
553 chemoattractant. Cells were allowed to invade for 24 h. After incubation, non-invading
554 cells were removed from the upper surface and cells on the lower surface were fixed
555 and stained with Diff-Quik kit (BD Biosciences). Membranes were photographed and
556 the invading cells were counted under a light microscope. Mean values from three
557 independent assays were calculated.

558

559 **4. Conclusion**

560

561 The present study has shown that these metal complexes with biologically active Schiff
562 base ligand offer an access to multi-targeted anticancer drugs, where most of the
563 observed biological activities are metal-dependent. It is noteworthy that metal ions play
564 a vital role in enhancing the biological activity of these complexes. Cu(II) complex **2**
565 exhibited the strongest topo I inhibition activity, DNA cleavage, and cytotoxicity, while
566 Zn(II) complex **1** showed better DNA binding activity, whereas Ni(II) complex **3**
567 possesses greater anti-invasion activity. The report of Zn(II), Cu(II), and Ni(II)
568 complexes with antimetastatic property is rare in the literature. Furthermore, the
569 outstanding antimetastatic property of the Ni(II) complex in contrast to its cytotoxicity

570 has convinced us that the fate of a compound should not be only dictated by its
571 cytotoxicity.

572

573

574 Acknowledgement

575

576 The authors would like to thank MOHE (FRGS-FP016-2013A, UM.C/625/1/HIR/247,
577 PPP-PG007-2012B) for supporting this study. We would like to thank Prof. Wong C.S.
578 and Prof. Norhanom W. for the use of their facilities.

579

580

581 References

582

- 583 1. M. L. Rothenberg, *Ann. Oncol.*, 1997, **8**, 837-855.
- 584 2. H. L. Seng, S. T. Von, K. W. Tan, M. J. Maah, S. W. Ng, R. N. Z. R. A. Rahman, I. Caracelli
585 and C. H. Ng, *BioMetals*, 2010, **23**, 99-118.
- 586 3. Y. C. Liu, Z. F. Chen, L. M. Liu, Y. Peng, X. Hong, B. Yang, H. G. Liu, H. Liang and C. Orvig,
587 *Dalton Trans.*, 2009, 10813-10823.
- 588 4. B. M. Zeglis, V. Divilov and J. S. Lewis, *J. Med. Chem.*, 2011, **54**, 2391-2398.
- 589 5. D. Palanimuthu, S. V. Shinde, K. Somasundaram and A. G. Samuelson, *J. Med. Chem.*,
590 2013, **56**, 722-734.
- 591 6. P. Katkar, A. Coletta, S. Castelli, G. L. Sabino, R. A. A. Couto, A. M. Da Costa Ferreira and
592 A. Desideri, *Metallomics*, 2014, **6**, 117-125.
- 593 7. K. W. Tan, H. L. Seng, F. S. Lim, S. C. Cheah, C. H. Ng, K. S. Koo, M. R. Mustafa, S. W. Ng
594 and M. J. Maah, *Polyhedron*, 2012, **38**, 275-284.
- 595 8. M. C. Rodríguez-Argüelles, M. B. Ferrari, F. Bisceglie, C. Pelizzi, G. Pelosi, S. Pinelli and
596 M. Sassi, *J. Inorg. Biochem.*, 2004, **98**, 313-321.
- 597 9. D. M. Kong, J. Wang, L. N. Zhu, Y. W. Jin, X. Z. Li, H. X. Shen and H. F. Mi, *J. Inorg.*
598 *Biochem.*, 2008, **102**, 824-832.
- 599 10. A. Silvestri, G. Barone, G. Ruisi, D. Anselmo, S. Riela and V. T. Liveri, *J. Inorg. Biochem.*,
600 2007, **101**, 841-848.
- 601 11. G. Barone, N. Gambino, A. Ruggirello, A. Silvestri, A. Terenzi and V. T. Liveri, *J. Inorg.*
602 *Biochem.*, 2009, **103**, 731-737.
- 603 12. S. T. Chew, K. M. Lo, S. K. Lee, M. P. Heng, W. Y. Teoh, K. S. Sim and K. W. Tan, *Eur. J.*
604 *Med. Chem.*, 2014, **76**, 397-407.
- 605 13. S. K. Lee, K. W. Tan, S. W. Ng, K. K. Ooi, K. P. Ang and M. A. Abdah, *Spectrochim. Acta,*
606 *Part A*, 2014, **121**, 101-108.
- 607 14. A. Masta, P. J. Gray and D. R. Phillips, *Nucleic Acids Res.*, 1995, **23**, 3508-3515.
- 608 15. E. S. Newlands, M. F. G. Stevens, S. R. Wedge, R. T. Wheelhouse and C. Brock, *Cancer*
609 *Treat. Rev.*, 1997, **23**, 35-61.
- 610 16. U. Schatzschneider and J. K. Barton, *J. Am. Chem. Soc.*, 2004, **126**, 8630-8631.
- 611 17. P. Zabierowski, J. Szklarzewicz, K. Kurpiewska, K. Lewiński and W. Nitek, *Polyhedron*,
612 2013, **49**, 74-83.
- 613 18. L. Z. Li, C. Zhao, T. Xu, H. W. Ji, Y. H. Yu, G. Q. Guo and H. Chao, *J. Inorg. Biochem.*, 2005,
614 **99**, 1076-1082.
- 615 19. A. A. El-Sherif and T. M. A. Eldebss, *Spectrochim. Acta, Part A*, 2011, **79**, 1803-1814.
- 616 20. G. Grivani, A. D. Khalaji, V. Tahmasebi, K. Gotoh and H. Ishida, *Polyhedron*, 2012, **31**,
617 265-271.
- 618 21. L. Casella and M. Gullotti, *J. Am. Chem. Soc.*, 1981, **103**, 6338-6347.
- 619 22. A. M. Farag, T. S. Guan, H. Osman, A. M. S. A. Majid, M. A. Iqbal and M. B. K. Ahamed,
620 *Med. Chem. Res*, 2013, **22**, 4727-4736.
- 621 23. A. Haikarainen, J. Sipilä, P. Pietikäinen, A. Pajunen and I. Mutikainen, *J. Chem. Soc.,*
622 *Dalton Trans.*, 2001, 991-995.

- 623 24. D. M. Boghaei and E. Askarizadeh, *Journal of Coordination Chemistry*, 2008, **61**, 1917-
624 1926.
- 625 25. A. W. Williamson, *Q. J. Chem. Soc.*, 1852, **4**, 229-239.
- 626 26. V. Bethmont, F. Fache and M. Lemaire, *Tetrahedron Lett.*, 1995, **36**, 4235-4236.
- 627 27. S. Saha, R. K. Kottalanka, P. Bhowmik, S. Jana, K. Harms, T. K. Panda, S. Chattopadhyay
628 and H. P. Nayek, *J. Mol. Struct.*, 2014, **1061**, 26-31.
- 629 28. D. B. Yadav, G. L. Morgans, B. A. Aderibigbe, L. G. Madeley, M. A. Fernandes, J. P.
630 Michael, C. B. De Koning and W. A. L. Van Otterlo, *Tetrahedron*, 2011, **67**, 2991-2997.
- 631 29. B. Basavaraju, H. S. Bhojya Naik and M. C. Prabhakara, *Bioinorg. Chem. Appl.*, 2007,
632 **2007**, 36497.
- 633 30. K. Samanta, B. Chakravarti, J. K. Mishra, S. K. D. Dwivedi, L. V. Nayak, P. Choudhry, H. K.
634 Bid, R. Konwar, N. Chattopadhyay and G. Panda, *Bioorg. Med. Chem. Lett.*, 2010, **20**,
635 283-287.
- 636 31. P. A. Duckworth, F. S. Stephens, K. P. Wainwright, K. D. V. Weerasuria and S. B. Wild,
637 *Inorg. Chem.*, 1989, **28**, 4531-4535.
- 638 32. A. Werner, *Z. Anorg. Allg. Chem.*, 1893, **3**, 267-330.
- 639 33. B. J. Coe and S. J. Glenwright, *Coord. Chem. Rev.*, 2000, **203**, 5-80.
- 640 34. X. Sheng, X. M. Lu, J. J. Zhang, Y. T. Chen, G. Y. Lu, Y. Shao, F. Liu and Q. Xu, *J. Org.*
641 *Chem.*, 2007, **72**, 1799-1802.
- 642 35. N. Shahabadi, S. Kashanian and F. Darabi, *Eur. J. Med. Chem.*, 2010, **45**, 4239-4245.
- 643 36. J. Hernandez-Gil, S. Ferrer, E. Salvador, J. Calvo, E. Garcia-Espana and J. C. Mareque-
644 Rivas, *Chem. Commun.*, 2013, **49**, 3655-3657.
- 645 37. M. W. Göbel, J. W. Bats and G. Dürner, *Angew. Chem. Int. Ed.*, 1992, **31**, 207-209.
- 646 38. U. Scheffer, A. Strick, V. Ludwig, S. Peter, E. Kalden and M. W. Göbel, *J. Am. Chem. Soc.*,
647 2005, **127**, 2211-2217.
- 648 39. C. Li, F. Zhao, Y. Huang, X. Liu, Y. Liu, R. Qiao and Y. Zhao, *Bioconjugate Chem.*, 2012, **23**,
649 1832-1837.
- 650 40. S. S. Tonde, A. S. Kumbhar, S. B. Padhye and R. J. Butcher, *J. Inorg. Biochem.*, 2006, **100**,
651 51-57.
- 652 41. P. U. Maheswari, S. Roy, H. Den Dulk, S. Barends, G. Van Wezel, B. Kozlevčar, P. Gamez
653 and J. Reedijk, *J. Am. Chem. Soc.*, 2006, **128**, 710-711.
- 654 42. H. L. Seng, H. K. A. Ong, R. N. Z. R. A. Rahman, B. M. Yamin, E. R. T. Tiekink, K. W. Tan,
655 M. J. Maah, I. Caracelli and C. H. Ng, *J. Inorg. Biochem.*, 2008, **102**, 1997-2011.
- 656 43. P. A. N. Reddy, M. Nethaji and A. R. Chakravarty, *Eur. J. Inorg. Chem.*, 2004, 1440-1446.
- 657 44. S. Anbu, M. Kandaswamy and B. Varghese, *Dalton Trans.*, 2010, **39**, 3823-3832.
- 658 45. N. H. Khan, N. Pandya, K. J. Prathap, R. I. Kureshy, S. H. R. Abdi, S. Mishra and H. C.
659 Bajaj, *Spectrochim. Acta, Part A*, 2011, **81**, 199-208.
- 660 46. R. Eshkourfu, B. Čobeljić, M. Vujčić, I. Turel, A. Pevec, K. Sepčić, M. Zec, S. Radulović, T.
661 Srdić-Radić, D. Mitić, K. Andjelković and D. Sladić, *J. Inorg. Biochem.*, 2011, **105**, 1196-
662 1203.
- 663 47. P. Tamil Selvi, H. Stoeckli-Evans and M. Palaniandavar, *J. Inorg. Biochem.*, 2005, **99**,
664 2110-2118.
- 665 48. B. L. Fei, W. S. Xu, H. W. Tao, W. Li, Y. Zhang, J. Y. Long, Q. B. Liu, B. Xia and W. Y. Sun, *J.*
666 *Photochem. Photobio. B*, 2014, **132**, 36-44.
- 667 49. J. B. Lepecq and C. Paoletti, *J. Mol. Biol.*, 1967, **27**, 87-106.
- 668 50. A. E. Friedman, J. C. Chambron, J. P. Sauvage, N. J. Turro and J. K. Barton, *J. Am. Chem.*
669 *Soc.*, 1990, **112**, 4960-4962.
- 670 51. K. E. Erkkila, D. T. Odom and J. K. Barton, *Chem. Rev.*, 1999, **99**, 2777-2796.
- 671 52. D. H. Tjahjono, S. Mima, T. Akutsu, N. Yoshioka and H. Inoue, *J. Inorg. Biochem.*, 2001,
672 **85**, 219-228.
- 673 53. G. Barone, A. Terenzi, A. Lauria, A. M. Almerico, J. M. Leal, N. Busto and B. García,
674 *Coord. Chem. Rev.*, 2013, **257**, 2848-2862.
- 675 54. P. Feng, T. L. Li, Z. X. Guan, R. B. Franklin and L. C. Costello, *Prostate*, 2002, **52**, 311-318.
- 676 55. R. B. Franklin and L. C. Costello, *Arch. Biochem. Biophys.*, 2007, **463**, 211-217.

- 677 56. T. D. Pfister, W. C. Reinhold, K. Agama, S. Gupta, S. A. Khin, R. J. Kinders, R. E.
678 Parchment, J. E. Tomaszewski, J. H. Doroshov and Y. Pommier, *Mol. Cancer Ther.*,
679 2009, **8**, 1878-1884.
- 680 57. K. Lang, T. L. Drell IV, K. S. Zaenker and F. Entschladen, *Recent Pat. Anti-Cancer Drug*
681 *Discov.*, 2006, **1**, 69-80.
- 682 58. S. Das, S. Sinha, R. Britto, K. Somasundaram and A. G. Samuelson, *J. Inorg. Biochem.*,
683 2010, **104**, 93-104.
- 684 59. D. A. Medvetz, K. D. Stakleff, T. Schreiber, P. D. Custer, K. Hindi, M. J. Panzner, D. D.
685 Blanco, M. J. Taschner, C. A. Tessier and W. J. Youngs, *J. Med. Chem.*, 2007, **50**, 1703-
686 1706.
- 687 60. V. Kolenko, E. Teper, A. Kutikov and R. Uzzo, *Nat. Rev. Urol.*, 2013, **10**, 219-226.
- 688 61. H. N. Keer, F. D. Gaylis, J. M. Kozlowski, H. C. Kwaan, K. D. Bauer, A. A. Sinha and M. J.
689 Wilson, *Prostate*, 1991, **18**, 201-214.
- 690 62. A. Levina, A. Mitra and P. A. Lay, *Metallomics*, 2009, **1**, 458-470.
- 691 63. A. Bergamo and G. Sava, *Dalton Trans.*, 2007, 1267-1272.
- 692 64. M. Zec, T. Srdic-Rajic, A. Konic-Ristic, T. Todorovic, K. Andjelkovic, I. Filipovic-Ljeskovic
693 and S. Radulovic, *Anti-Cancer Agents Med. Chem.*, 2012, **12**, 1071-1080.
- 694 65. G. M. Sheldrick, *Acta Cryst. A*, 2007, **64**, 112-122.
- 695 66. L. J. Barbour, *J. Supramol. Chem.*, 2001, **1**, 189-191.
- 696 67. W. Xu, X. Yang, L. Yang, Z. L. Jia, L. Wei, F. Liu and G. Y. Lu, *New J. Chem.*, 2010, **34**,
697 2654-2661.
- 698 68. L. Liu, G.-M. Zhang, R.-G. Zhu, Y.-H. Liu, H.-M. Yao and Z.-B. Han, *RSC Adv.*, 2014, **4**,
699 46639-46645.
- 700 69. C. K. Mirabelli, C. H. Huang and S. T. Crooke, *Cancer Res.*, 1980, **40**, 4173-4177.
- 701 70. R. P. Hertzberg and P. B. Dervan, *J. Am. Chem. Soc.*, 1982, **104**, 313-315.
- 702 71. A. M. Pyle, J. P. Rehmann, R. Meshoyrer, C. V. Kumar, N. J. Turro and J. K. Barton, *J. Am.*
703 *Chem. Soc.*, 1989, **111**, 3051-3058.
- 704 72. A. Wolfe, G. H. Shimer Jr and T. Meehan, *Biochemistry*, 1987, **26**, 6392-6396.
- 705
- 706